Photoassembly of the Manganese Cluster in Mutants Perturbed in the High Affinity Mn-Binding Site of the H_2O-Oxidation Complex of Photosystem II†

Hong Jin Hwang,‡ Aaron McLain,‡ Richard J. Debus,# and Robert L. Burnap*,‡

Department of Microbiology and Molecular Genetics, Oklahoma State University, Stillwater, Oklahoma 74078, and Department of Biochemistry, University of California, Riverside, California 92521

Received April 23, 2007; Revised Manuscript Received September 17, 2007

ABSTRACT: The light-driven, oxidative assembly of Mn^{2+} ions into the H_2O-oxidation complex (WOC) of the photosystem II (PSII) reaction center is termed photoactivation and culminates in the formation of the oxygen-evolving (Mn_4−Ca) center of the WOC. Initial binding and photooxidation of Mn^{2+} to the apoprotein is critically dependent upon aspartate 170 of the D1 protein (D1−D170) of the high affinity Mn site [Nixon and Diner (1992) *Biochemistry 31*, 942−948]. Three O_2-evolving mutant strains of *Synechocystis*, D1−D170E, D1−D170H, and D1−D170V, were studied in terms of the kinetics of photoactivation under both continuous and flashing light. Photoactivation using single turnover flashes revealed D1−D170H and D1−D170V, but not D1−D170E, were prone to form substantial amounts (∼40−50%) of inactive centers ascribed to photoligation of aberrant nonfunctional Mn based upon the reversibility of the inactivation and similarity to previous *in vitro* results [Chen, C., Kazimir, J., and Cheniae, G. M. (1995) *Biochemistry 34*, 13511−13526]. On the other hand, D1−D170E lowers the quantum efficiency of photoactivation compared to the wild-type by the largest amount (80% decrease) versus D1−D170H and D1−D170V, which do not produce measurable decreases in quantum efficiency. The low quantum efficiency of photoactivation in D1−D170E is due to the destabilization of photoactivation intermediates. Numerical analysis indicates that the PSII centers in D1−D170E are heterogeneous with respect to photoactivation kinetics and that the majority of centers are characterized by intermediates that decay ∼10-fold more rapidly than the wild-type control. Additionally, the kinetics of O_2 release during the S_3−S_0 transition was markedly retarded in D1-D170E, in contrast to D1-D170H and D1-D170V, which did not exhibit a discernible slow-down compared to the wild-type.

The photosystem II (PSII[1]) reaction center of oxygenic photosynthesis catalyzes the highly endergonic transfer of electrons from water to plastoquinone using light as a source of energy. The structure of the PSII complex has been determined up to a resolution of about 3.0 Å using X-ray diffraction (*1*−*4*). Photooxidized primary donor, $P680^+$, is a powerful oxidant capable of extracting the tightly bound electrons of substrate H_2O bound to the water-oxidation complex (WOC) via the redox active tyrosine, Y_Z, of the D1 protein. Since the oxidation of the two substrate H_2O to O_2 is a four-electron process, four successive charge separations are required as the WOC transits through a series of oxidation states, designated S_0 through S_3, during the catalytic cycle of H_2O oxidation.

The photooxidant $P680^+$ also serves another crucial and related function: oxidizing Mn^{2+} ions during the assembly of the WOC. The Mn_4−Ca of the WOC is necessarily formed via an oxidative mechanism involving the photooxidation of Mn^{2+} ions bound to the apo-coordination environment of the PSII complex. Thus, in addition to driving the removal of electrons from H_2O bound during the catalytic cycle, $P680^+$ is also utilized as the primary photooxidant, extracting electrons from Mn^{2+}, again via Y_Z, during formation of the Mn_4−Ca catalytic center. The assembly of the Mn_4−Ca is thus a light-dependent process termed photoactivation (reviewed in refs *5*, *6*). The intermediates in the photoassembly of the PSII Mn_4−Ca have only limited kinetic stability, which accounts for the low yields of O_2-evolving activity when photoactivation is promoted by flashes given to Mn-extracted samples at long intervals between flashes (>2 s) (*7*−*10*). On the other hand, flashes given with very short intervals are also not optimal because of a rate-limiting dark process ($t_{1/2}$ ∼150 ms) that must go to completion between flashes. The combination of these opposing kinetic features results in a 'bell-shaped' curve when the yield of photoactivation due to a finite number of flashes is plotted as a function of the time interval between the photoactivating flashes (*7*, *8*, *11*, *12*). These features have been described by a "two-quantum series model" (*10*, *12*−*19*) as depicted in Scheme 1. The model posits that two distinct photoact, **A** ⟹ **B** and **C** ⟹ **D**, are required to form the first stable intermediate state, **D**, in the assembly pathway leading to the formation of an active O_2-evolving Mn_4−Ca. The stable intermediate is suggested to be a binuclear Mn^{3+}−Mn^{3+} species (*13*, *20*, *21*). Following the first photoact, **A** ⟹ **B**, a refractory

† This work was funded by the National Science Foundation (MCB-0448567 to R.L.B.) and the National Institutes of Health (GM-076232 to R.J.D).

* Corresponding author. Phone: 405-744-7445, Fax: 405-744-6790, e-mail: burnap@biochem.okstate.edu.

‡ Oklahoma State University.

University of California.

[1] Abbreviations: Chl, chlorophyll; DCBQ, 2,6-dichrlorobenzoquinone; EDTA, (ethylenedinitrilo)tetraacetic acid; HA, hydroxylamine (NH_2OH); HEPES, 4-(2-hydroxyethyl)-1-piperazineethanesulfonic acid; HBG-11, normal BG-11 growth medium buffered with HEPES−NaOH pH 8; PSII, photosystem II; WOC, H_2O oxidation complex of PSII; XRD, x-ray diffraction.

10.1021/bi700761v CCC: $37.00
Published on Web 11/02/2007

Scheme 1

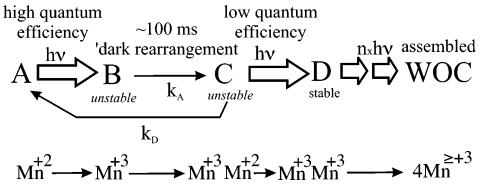

period, represented in the model by the light-independent process **B** ⇒ **C** ($t_{1/2}$ ~100 ms), must elapse before the next quantum can be productively utilized to drive the second photoact, **C** ⇒ **D**. The overall quantum efficiency of photoactivation is very low (≪0.01), and it is thought that the initial photooxidation (**A** ⇒ **B**) occurs with relatively high quantum efficiency, whereas the second photoact (**C** ⇒ **D**) accounts for the very low overall quantum efficiency. The nature light-independent process **B** ⇒ **C**, referred to as the 'dark rearrangement', is not established although mechanisms involving protein conformational or charge rearrangements have not been excluded.

Although the nature of late intermediates of photoactivation remains obscure, there is definitive information on the initial assembly intermediate, simplistically represented as **A** ⇒ **B** in the two-quantum model. The initial event involves the binding and photooxidation of a single Mn^{2+} ion to the high affinity site of PSII (*22*). Ananyev and colleagues provided evidence that the Mn species bound within the high affinity site is the hydroxide, $[Mn-OH]^{1+}$ (*23*), consistent with the observation that one proton is released upon binding Mn^{2+} to the high affinity site (*24*). As mentioned, this step occurs with high quantum efficiency (at least higher than subsequent Mn^{2+} photooxidations (*13*, *17*, *25*, *26*)), although estimating this quantum yield is complicated by difficulty in assaying this event and the binding dynamics of Mn^{2+} at the high affinity site (*27*−*29*). Site-directed mutagenesis has identified aspartate 170 of the D1 protein (D1−D170) as being the most critical residue for the PSII high affinity Mn site examined to date (*30*, *31*), which is consistent with X-ray diffraction crystallographic models of the PSII complex (*1*, *3*). Recent studies have established that other D1 amino acid residues that are likely ligands of the Mn_4−Ca also have a strong influence on the binding affinity of the single Mn^{2+} ion to the high affinity site. The results were interpreted in terms of an electrostatic contribution by increasing the local concentration of Mn^{2+} in the vicinity of the high affinity site and indicate that the D1 conformation of the Mn-free protein site has already adopted a configuration similar to the D1 fold of the functioning enzyme thereby ruling out the possibility that large-scale structural rearrangements accompany Mn_4−Ca assembly (*32*).

In this study we have investigated the photoactivation properties of mutants with substitutions of D1−D170 in the high affinity site of PSII. These mutants, involve substitutions of the aspartate with glutamate, histidine, and valine (D1−D170E, D1−D170H, and D1−D170V) and are capable of evolving O_2, albeit at impaired rates (*30*, *31*, *33*, *34*). Importantly, information on the ability (K_m) of Mn^{2+} to reduce $Y_Z^{\oplus}$ is available for two of the three mutants investigated (*31*, *35*). As these mutants were previously assessed as having impaired assembly of the Mn_4−Ca (*30*, *31*, *33*, *34*), a further analysis of their photoactivation characteristics was conducted.

MATERIALS AND METHODS

Strains and Growth Conditions. The glucose-tolerant strain of *Synechocystis* sp. PCC6803 isolated by Williams and the PSII mutant derivatives were routinely maintained in BG-11 medium as described previously (*36*). Experimental cultures were propagated in BG-11 media buffered with 20 mM HEPES−NaOH pH 8.0 (HBG-11) with 5 mM glucose and under PFD (photon flux density) of ~70 μmol m^{-2} s^{-1} at 30 °C. Cultures were bubbled with filter-sterilized air enriched with 3% CO_2. The strains were previously characterized with respect to their growth under photoautotrophic and photoheterotrophic conditions (Chu et al. 1994). The strains were harvested for experiments in late logarithmic growth phase (O.D.750 nm ~1.2) when the level of PSII activity, judged by variable fluorescence, was maximal for all strains examined here (see below). Light intensity measurements were made with a LiCor sensor (Lincoln, NE). Construction and characterization of the D1−D170E, D1−D170H, and D1−D170V strains were performed as previously (Chu et al. 1994) using the *psbA2*-containing plasmid pRD1031 and the triple *psbA* deletion strain 4E-3. The strain designated WT* served as a control strain and was obtained by transformation of the triple deletion stain, 4E-3, with plasmid pRD1031 which contains wild-type *psbA2* (Chu et al. 1994).

Hydroxylamine Extraction of Cells. When cultures were in late-log phase and variable fluorescence ($(F_m - F_0)/F_0$) measured with a PAM fluorometer (Walz Inc.) of the cultures were over 0.2 (D1−D170V), 0.3 (D1−D170H and D1−D170E), or 0.6 (WT*), approximately 400 mL of cells was pelleted at 25 °C at 5850*g* (Sorvall, GSA rotor) for 10 min. Hydroxylamine (HA) extraction to remove PSII Mn was conducted as described previously (*8*, *9*, *17*). To address the potential issue of different degrees of extraction in mutants, preliminary experiments used 10-fold higher HA concentrations (10 mM versus 1 mM), and while increased washing was required to remove residual amounts of HA that interfered with photoactivation, the quantum efficiencies of O_2 evolution restoration were essentially the same although final yields were reduced ~20−30% presumably due to irreversible damage caused at high HA concentrations.

Photoactivation of HA-Extracted Cells. HA-extracted cells were photoactivated using the previously described experimental setup (*9*, *17*). At the completion of the photoactivation flash treatment, 100 μL aliquots (100 μg Chl mL^{-1}) were withdrawn for assay for light-saturated rates of O_2 evolution, which were determined using a Clark-type electrode. Photoactivated samples were resuspended in HN (10 mM HEPES, pH 7.2, 30 mM NaCl) buffer supplemented with an artificial electron acceptor system consisting of 1 mM DCBQ and 1 mM potassium ferricyanide, and oxygen evolution was measured in response to saturating orange (>570 nm) illumination at 30 °C. Experiments measuring the development of O_2 evolution as a function of single-turnover flash number (Figure 2) provide information on the quantum efficiency of photoactivation which is reflected in the initial slope of the curve. This permits estimation of the per flash quantum efficiency by fitting the data, assuming an exponential decrease in the number of centers remaining to be photoactivated in a population of (PSII) reaction center undergoing photoactivation (*11*, *17*). Estimation of the

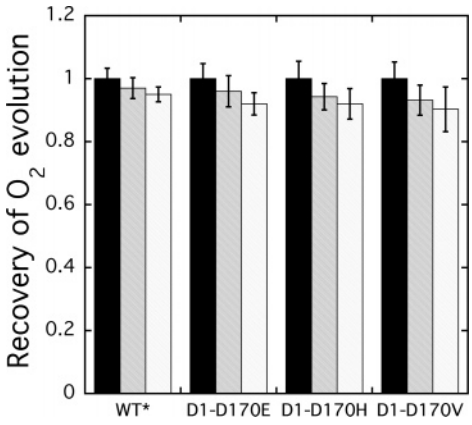

FIGURE 1: Recovery of light-saturated O_2-evolving activity of HA-extracted mutant and control cells exposed to continuous illumination. Cells were extracted with HA and placed under illumination ($\sim$20 μmol m^{-2} s^{-1}) while being gently agitated on a rotary shaker and assayed for maximal O_2-evolving activity. All the strains except D1−D170E reached maximal activity within 15 min under these conditions. The similarly treated D1−D170E strain reached maximal activity after approximately 40 min. Original O_2-evolving activities prior to HA-extraction were: 710 ± 23, 372 ± 17, 364 ± 20, and 242 ± 13 μmol O_2 (mg Chl) $^{-1}$ h^{-1}, for WT*, D1−D170E, D1−D170H, and D1−D170V, respectively. Error bars represent standard deviations, $n \geq 3$.

parameters specifying the dark rearrangement, k_A, and the decay of intermediates, k_D, was determined by evaluating the rising and falling slopes of the bell-shaped curve, respectively, in plots of photoactivation yield as a function of flash interval (Figure 3) which was done by fitting the data to the equation (*10*, *13*):

$$Y_n = [k_A/(k_D - k_A)][A1](e^{-k_A td} - e^{-k_D td}) \quad (1)$$

Here, Y_n is the yield of active centers on the nth flash, A1, is the concentration of centers prior to the photoactivation, and the other parameters have meanings described as in Scheme 1. Fitting to this equation gave estimates for k_A and k_D, as well as A1. A1 depends upon the quantum efficiency such that A1= $\Phi[D]_0$, where Φ is the overall photoactivation process. Note that the number of flashes is not explicitly taken into account fitting, and instead the experiments are conducted with the number of flashes set to give approximately 50% recovery of activity (see legends of Figure 3 and Table 1) to allow a rough comparison of the fitted values of A1. For the D1−D170E mutant, it was found that the results of the flash interval experiment were best fit by assuming that cells contained a mixture of apo-centers composed of wild-type and modified characteristics. This situation was modeled by the following equation:

$$Y_n = [k_{A1}/(k_{D1} - k_{A1})][A1](e^{-k_{A1} td} - e^{-k_{D1} td}) + [k_{A2}/(k_{D2} - k_{A2})][A2](e^{-k_{A2} td} - e^{-k_{D2} td}) \quad (2)$$

Oxygen Rate Electrode Measurements. Flash O_2 yields were performed using a bare platinum electrode that permits the centrifugal deposition of membrane fragments upon the electrode surface (*31*), according to a previously described procedure (*37*, *38*). Care was taken to apply equal amounts of sample and at a minimal amount to minimize the path of diffusion to the electrode surface (*39*−*42*). With such care, the 1.2 ms O_2 release kinetic can be resolved in wild-type samples (Figure 5). These measurements approximately track the relative amounts of O_2 release of each number of a flash under a train of flashes and thereby provide information on the distribution of S-states populated in dark-adapted samples and the kinetics of the O_2 signal. Analysis of the oscillatory pattern of O_2 release from dark adapted samples subject to a train of flashes was performed according to a four-state model (*43*).

RESULTS

Photoactivation of Hydroxylamine-Treated Cells under Continuous Light. The aspartate 170 of the D1 protein (D1−D170) has been shown to be crucial residue for photooxidation of Mn^{2+} via binding at the high affinity site Mn of PSII (*30*−*32*, *44*). Extensive analysis of mutations at this site have previously been shown to perturb both the K_m of reduction of $Y_Z^{\bullet}$ by Mn^{2+} in apo-PSII and the ability of reaction centers to assemble O_2-evolving Mn_4−Ca clusters (*30*−*32*, *44*). Here, three strains of *Synechocystis* with substitution mutations at this critical position were studied with regard to their photoactivation properties: D1−D170E, D1−D170H, and D1−D170V. These strains were previously constructed using a deletion strain of *Synechocystis*, designated 4E-3, that lacks all three native copies of the *psbA* gene (*psbA1*, *psbA2*, and *psbA3*) and which was transformed with mutant forms of the *psbA2* gene to introduce the desired mutations into the otherwise normal *Synechocystis* PSII complex (*45*). A control strain, WT*, was constructed identically to the mutants, but using the wild-type *psbA2* sequence. The D1−D170E, D1−D170H, and D1−D170V strains all evolve oxygen, although at impaired rates relative to the control (*30*, *31*, *44*, *46*). Initial experiments were performed to evaluate these strain in terms of their ability to reassemble O_2-evolving Mn clusters following their extraction using hydroxylamine (HA), which completely abolishes O_2-evolution (*7*, *9*, *11*). Figure 1 documents the net recovery of light-saturated, DCBQ-supported, O_2-evolving activity of a suspension of HA-extracted mutant and control cells exposed to continuous illumination ($\sim$20 μmol m^{-2} s^{-1}), while being gently agitated on a rotary shaker. These low light levels are optimal because, as noted earlier (*7*, *9*, *11*), the rate-limiting step(s) of photoactivation preclude the productive utilization of excitons arriving at higher rates into the reaction center. All the strains except D1−D170E reached maximal activity within 10−15 min under these conditions. The similarly treated D1−D170E strain reached maximal activity after approximately 30−40 min. The level of recovery (Figure 1, gray bars) exceeded greater than 95% of the original activity (black bars) in the control, WT*, whereas the level of O_2-evolution activity was restored to 85−95% of the original activity (black bars) in the mutant strains. The recoveries are expressed as the fraction of the rate prior to HA-extraction. The actual rates of O_2-evolution prior to HA-extraction, which are given in the figure legends, are consistent with previous values (*30*, *31*, *44*, *46*). When the cycle of HA-extraction and photoactivation was repeated, the fractional recovery of activity by photoactivation under continuous illumination was again high, with some small ($\sim$5%) apparently irretrievable losses (Figure 1, light bars). In conclusion, all HA-extracted strains exhibited very high photoactivation recoveries of O_2-evolution activity under

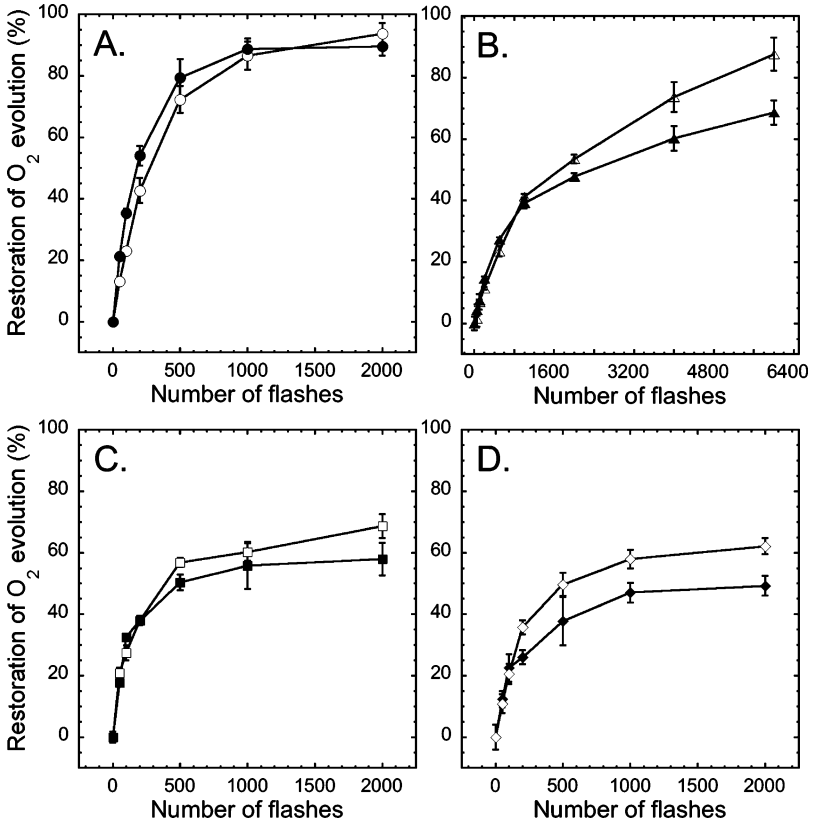

FIGURE 2: Photoactivation of hydroxylamine-extracted cells as a function of the number of flashes. Note the difference in scale of D170E (Panel B). Sequences of photoactivating xenon flashes were given with a uniform interval of 0.5 s to HA-extracted WT* (Panel A), D1−D170E (Panel B), D1−D170H (Panel C), and D1−D170V (Panel D) cells in the presence (closed symbols) or absence (open symbols) of 50 μM DCBQ plus 200 μM of potassium ferricyanide. The recoveries are expressed in terms of the original O_2-evolving activities of the corresponding cells prior to HA-extraction which were 739 ± 20, 364 ± 19, 335 ± 20, and 298 ± 13 μmol O_2 (mg Chl) $^{-1}$ h^{-1}, for WT*, D1−D170E, D1−D170H, and D1−D170V, respectively. Error bars represent standard deviations, $n \geq 3$.

continuous illumination, although D1−D170E required longer exposures to reach maximal recovery.

Flash Number Dependence Photoactivation. To obtain information on the effect of the substitution mutations on the quantum efficiency of photoactivation, cells were photoactivated using single-turnover flash illumination. Figure 2 shows the yields of photoactivation of HA-extracted cells as a function of flash number, where samples were subjected to a sequence of single turnover xenon flashes given at 2 Hz. During a train of xenon flashes given to WT* (open symbols Figure 2A), the development of O_2-evolution activity is nearly complete (>90%) relative to the initial starting activity within approximately 2000 flashes, as expected based on earlier findings with the true wild-type (*9*, *17*). The quantum efficiency of this process can be estimated from the initial slope of this curve, which reflects the per flash increment in the development of O_2-evolution activity. The quantum efficiency for the wild-type is approximately 3.0×10^{-3}, which is consistent with the low overall quantum efficiency of this process. In the presence of an artificial electron acceptor, DCBQ, the quantum efficiency is increased to 4.9×10^{-3} as demonstrated early in the flash sequence, while the final yield of recovered activity was slightly depressed (closed symbols Figure 2A). Compared to WT*, the D1−D170E mutant exhibited a far lower net quantum efficiency of photoactivation, requiring nearly 6000 flashes to reach levels approaching 90% of the original activity (open symbols Figure 2, Panel B). Correspondingly, the quantum efficiency is estimated to be 5.6×10^{-4} and 9.4×10^{-4} in the absence and presence of DCBQ, which is about 19% of the wild-type under comparable conditions. Even when the flash interval was shortened to 200 ms, which is near the optimum for this mutant (next section), the development of activity on a per flash basis was still much lower than WT* (not shown). Thus, the overall quantum efficiency of photoactivation is decreased 5-fold in D1−D170E.

In contrast to D1−D170E, both D1−D170V and D1−D170H reached a maximum yield of photoactivation in fewer than 1000 flashes. For D1−D170H, this corresponded to calculated quantum efficiencies of 5.7×10^{-3} and 6.8×10^{-3} in the absence and presence of DCBQ, respectively. Again, these calculated values reflect the per flash increment in the development of O_2-evolution activity. For D1−D170V, this corresponded to calculated quantum efficiencies of 3.3×10^{-3} and 4.1×10^{-3} in the absence and presence of DCBQ, respectively. These efficiencies are higher than the wild-type, but these numbers need to be treated with caution since another process ascribed to inactivation (below) causes these curves to reach a plateau at very low values. In fact, the final yield corresponded to a recovery of only 40−60% of the original activity, contrasting with the wild-type and D1−D170E, which exhibited nearly complete recoveries. As with the D1−D170E mutant, DCBQ depressed the final yield of O_2-evolving activity in D1−D170V and D1−D170H, but this depression was even more pronounced. In conclusion, a much lower recovery of O_2-evolving activity was obtained by flash photoactivation of D1−D170H and D1−D170V,

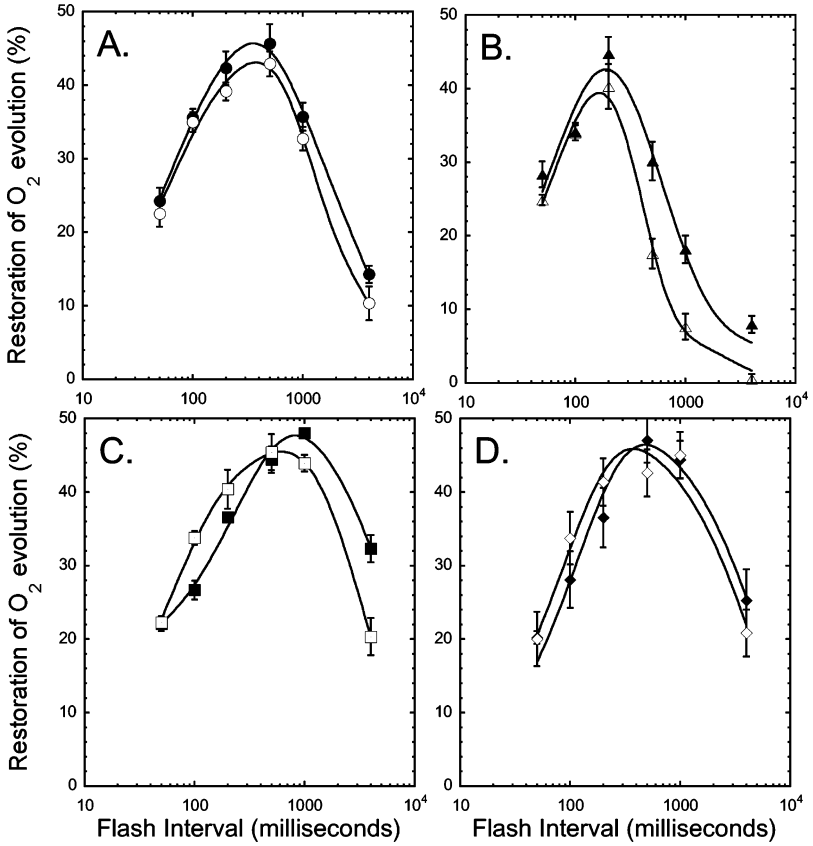

FIGURE 3: Photoactivation of HA-extracted WT* cells as a function of the flash interval. Flashes were given at six different equally spaced flashes given at different time intervals to HA-extracted WT* (Panel A), D1−D170E (Panel B), D1−D170H (Panel C), and D1−D170V (Panel D) cells in the presence (closed symbols) or absence (open symbols) of 50 μM DCBQ plus 200 μM of potassium ferricyanide. The curves represent fits to eqs 1 and 2 derived from the two-quantum model depicted in Scheme 1 (*10*). A homogeneous population of centers was assumed (eq 1) for all strains except D1−D170E, which was better fit by using eq 2 that assumes a heterogeneous population containing wild-type and modified centers. The number of flashes given were determined on the basis of preliminary flash number experiments (e.g., see Figure 2) so as to give approximately 50% restoration of activity at 5 Hz (D1−D170E) or 2 Hz for the other strains. This corresponded to 150, 200, 200, and 500 flashes for WT*, D1−D170V, D1−D170H, and D1−D170E, respectively. The recoveries are expressed in terms of the original O_2-evolving activities of the corresponding cells prior to HA-extraction which were 710 ± 23, 372 ± 17, 364 ± 20, and 242 ± 13 μmol O_2 (mg Chl)$^{-1}$ h^{-1}, for WT*, D1−D170E, D1−D170H, and D1−D170V, respectively. Error bars represent standard deviations, $n \geq 3$. Curves were fit according to the equations described in Materials and Methods.

Table 1: Dark Rearrangement, k_A, and Decay of Intermediates, k_D, Parameters[a] of the WT* and Mutant Strains of *Synechocystis* sp. PCC6803

strain	A1	k_{A1} (s^{-1}) ($t_{1/2}$)	k_{D1} (s^{-1}) ($t_{1/2}$)	A2	k_{A2} (s^{-1}) ($t_{1/2}$)	k_{D2} (s^{-1}) ($t_{1/2}$)	fit quality R
WT*	50	13 (54 ms)	0.330 (2.1 s)	na[b]	na	na	0.99
D1−D170E	23	13 (54 ms)	0.330 (2.1 s)	54	7 (95 ms)	5 (0.1 s)	0.99
D1−D170H	48	9 (78 ms)	0.097 (7.1 s)	na	na	na	0.96
D1−D170V	50	8 (85 ms)	0.174 (4.1 s)	na	na	na	0.99

[a] Values of parameters were estimated from fits of the flash interval experiment (Figure 3) using the equations derived (*10*) from the two-quantum model (Scheme 1) as presented in Materials and Methods. A homogeneous population of centers was assumed (eq 1) for all strains except D1-D170E, which was better fit by using eq 2 that assumes a heterogeneous population *s* containing wild-type and modified centers. Note that the number of photoactivating flashes were different among samples and were adjusted to produce approximately 50% restoration of activity at 5 Hz (D1−D170E) or 2 Hz for the other strains. This corresponded to 150, 200, 200, and 500 flashes for WT*, D1−D170V, D1−D170H, and D1−D170E, respectively. [b] Not applicable since the homogeneous model (eq 1) was sufficient to produce a reasonable fit.

in contrast to photoactivation under continuous illumination, where nearly complete recovery was obtained (Figure 1). The failure to reach levels of activity under flash illumination approaching the levels attained under continuous illumination indicates that D1−D170V and D1−D170H are prone to damage or inactivation under flash illumination. This observation is further explored later.

Yields of Photoactivation as a Function of Flash Interval. Photoactivation involves the formation of two unstable intermediates separated by a light-independent (dark) rearrangement step that has been estimated to occur with a ~100 ms half-time (Scheme 1). These kinetic features give rise to the bell-shaped curve in plots of the photoactivation yield as a function of flash interval obtained by measuring the extent of recovery of oxygen evolution due to a finite number of flashes given at different frequencies ranging from a few milliseconds to several seconds (*7*, *10*, *17*, *38*, *47*−*49*). This is illustrated in Figure 3, showing that the WT* and mutant strains all exhibit this characteristic flash interval dependence of photoactivation yield. In contrast to the other strains, D1−D170E (Figure 3, Panel B) was observed to have an optimal flash spacing of 200 ms compared to an optimum centered in the 500−1000 ms range for the other strains (Figure 3, Panels A, C, and D). This

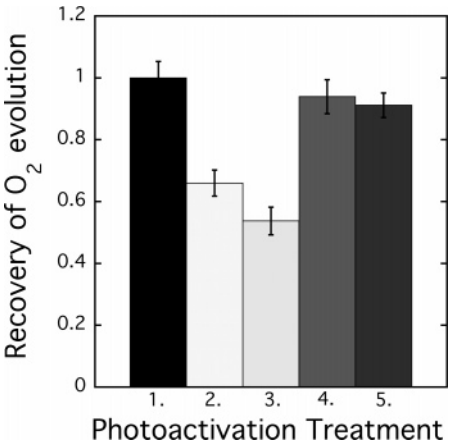

FIGURE 4: Photoinactivation occurring during flash photoactivation of D1−D170V is reversible. Cells of the D1−D170V strain were extracted with HA and photoactivated using single turnover flashes, in the absence (treatment 2) or presence of DCBQ/FeCN (treatment 3) and assayed for maximal O_2-evolving activity. Aliquots of the same flash photoactivated samples from treatments 2 and 3 were then re-extracted with HA, photoactivated under continuous illumination (~20 μmol m^{-2} s^{-1}) in the absence of artificial electron acceptors, and assayed for maximal O_2-evolving activity (treatments 4 and 5, respectively). Treatment 1 represents the original O_2-evolving activity D1−D170V cells prior to the first HA-extraction, which was 255 ± 14 μmol O_2 (mg Chl) $^{-1}$ h^{-1}. Error bars represent standard deviations, $n \geq 3$.

indicates that the labile photoactivation intermediates are considerably less stable in D1−D170E compared to the other strains. Decreased stability of photoactivation intermediates is consistent with the observation that the overall quantum efficiency of photoactivation is lower in D1−D170E as deduced from the flash number experiment shown in Figure 2. To evaluate this observation semiquantitatively, the flash interval data were fit to an equation derived from the two-quantum series model (Scheme 1) taking into account the dark-rearrangement parameter, k_A, and the decay of intermediate(s) parameter, k_D (*10*). The data of the wild-type and, to lesser extent, D1−D170H and D1−D170V are well-fit by this equation (Figure 3 and Table 1). The obtained values of k_A, k_D, and A1 (a product of the quantum yield of the whole process of photoactivation and the population of Mn-depleted PSII centers) in WT* centers are 12.91 s^{-1}, 0.33 s^{-1}, and 49.8%, respectively. Expressed in terms of half-times this corresponds to a dark rearrangement and decay of intermediates of 53.7 ms and 2.1 s, respectively. On the other hand, the data of D1−D170E are not well-fit to the simulation curve especially at longer flash intervals. However, if there are two heterogeneous apo-centers (a mixture of WT and modified type) in the mutant cells, the data are well fit to the corresponding simulation curve described by an equation taking into account this heterogeneity (see Materials and Methods). Values of the wild-type k_{A1} and k_{D1} (12.91 s^{-1}, 0.33 s^{-1}) were assumed for the WT*-type centers, while the fraction of each type of centers (reflected in parameters A1 and A2) and modified-type k_{A2} and k_{D2} were all allowed to range freely during the fitting to the data. As shown in Table 1, the half-times of k_{A2} and k_{D2} in the modified centers in D1−D170E were estimated to be 7.2 s^{-1} and 5.2 s^{-1}, respectively. The ratio of populations of modified to WT* ones may be approximately 10, considering that the quantum efficiency of the overall process is 5-fold higher in the WT*. The rate constant (k_A) of 'B' to 'C' is considerably smaller in the modified centers, while the rate constant (k_D) of 'C' to 'A' is significantly larger in the modified ones. In D1−D170H and D1−D170V, both values for k_A and k_D seem to be rather smaller than those of the wild-type.

Photoinactivation Occurring during Flash Photoactivation Is Reversible. The very low final recovery of O_2-evolving activity (~50−60%) in the mutants during flash photoactivation, especially in D1−D170V (Figure 2), was surprising considering that photoactivation under continuous illumination yielded activities approaching 90% of the original activity (Figure 1). These results suggest that flash illumination leads to an inactivation of more than 40% of the PSII centers, in an inactivation process that is exacerbated by the addition of DCBQ. Earlier studies have indicated that irreversible photodamage as well as reversible photoinactivation can account for diminished yields of photoactivation (*13*, *50*). To discriminate between these possibilities, the D1−D170V mutant was subjected to photoactivation with 2000 Xenon flashes, assayed for activity, re-extracted with HA, and then subjected to photoactivation under continuous illumination. As shown in Figure 5, photoactivation with 2000 xenon flashes in the absence or presence of DCBQ/FeCN (treatments 2 and 3, respectively) gave low yields of recovery consistent with the flash number experiment shown in Figure 2. However, upon re-extraction with HA followed by a second round of photoactivation, but this time using continuous light, most of the original activity could be recovered in these originally flash photoactivated and significantly photoinactivated samples (treatments 4 and 5). The addition of the protein synthesis inhibitor, lincomycin (200 μg/mL), had no influence on the extent of recovery either under continuous or flash illumination (not shown), so the differences between photoactivation by flash and continuous illumination cannot be ascribed to differences in the repair of damage to PSII. Therefore, we conclude that photoactivation under flash illumination results in a significant fraction of PSII centers becoming reversibly inactivated in a process that is exacerbated by the presence of an electron acceptor. Furthermore, the fact that re-extraction with hydroxylamine is required for the reversal of the inactivation suggests that inactivated centers contain photooxidized Mn that must be removed prior to the restoration of activity under continuous illumination.

Properties of the Assembled WOC: O_2 Evolution and S-State Cycling. To better evaluate differences in the S-state cycling and O_2 release characteristics of the assembled WOC, measurements of O_2 evolution of isolated membranes under flash illumination using centrifugal bare platinum electrode were performed. As shown previously, D1−D170E and D1−D170H exhibited characteristic period four oscillations in O_2 release (*31*), a property not unexpectedly shared by D1−D170V. The results of the flash O_2 evolution characteristics, summarized in Table 2, show that all mutants exhibited a somewhat increased value of misses contributing to the damping of the period four oscillations, denoted as the parameter, α. Surprisingly, the ostensibly most conservative replacement D1−D170E, not D1−D170V, appeared to have the greatest deviations from the control strain, and this divergence in catalysis was especially evident in the kinetics of O_2 release, as illustrated in Figure 5 and expressed numerically in the last column of Table 2. D1−D170E

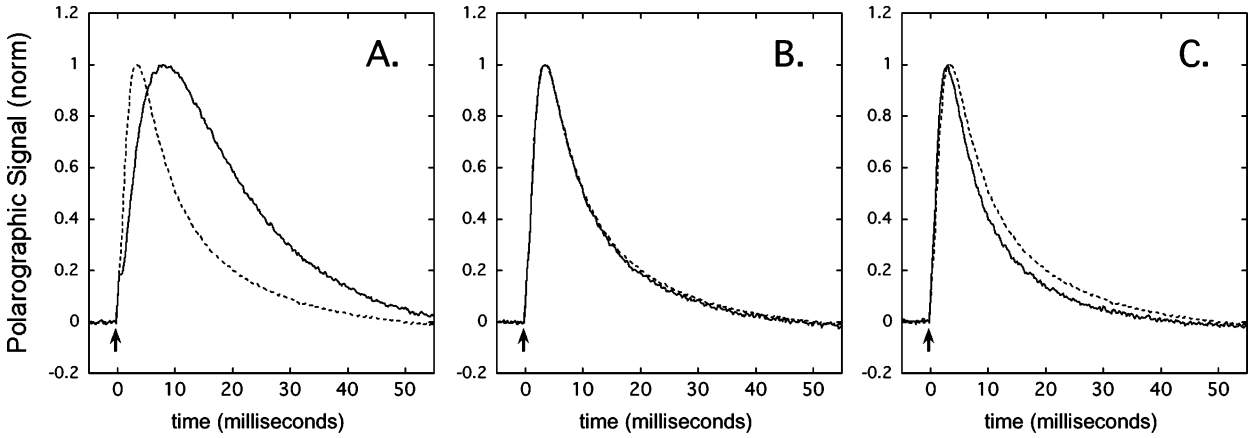

FIGURE 5: Oxygen signals of mutant and control membranes. The normalized flash-induced polarographic signals from D1−D170E, D1−D170H, and D1−D170V membranes (solid traces, Panels A−C, respectively) are compared with the corresponding signal of the WT* control (dashed trace in each panel). Membranes were centrifugally deposited upon the surface of a bare-platinum electrode and given a sequence (4 Hz) of 40 saturating xenon flashes and the signals averaged. Normalization was applied to allow a better comparison of the kinetics of O_2 appearance at the electrode surface and is not meant to indicate similar amounts of O_2 released per sample. The exponential half-rise times of the depicted signals are given in Table 2. Kinetic analysis of the data was performed according to the exponential method (*60*).

Table 2: S-State Decay Cycling Parameters of Oxygen-Evolving Membranes of the WT* and Mutant Strains of *Synechocystis* sp. PCC6803

strain	S-state distribution: $S_0/S_1/S_2/S_3$ (%)	misses, α (%)	hits, β (%)	double hits, γ (%)	deactivations, δ (%)	O_2 release[b] $t_{1/2}$, membranes (ms)
WT*	23/74/3/0	10	86	2	2	1.2
D1−D170E	28/68/4/0	14	80	2	4	5.6
D1−D170H	28/68/4/0	10	85	2	2	1.2
D1−D170V	23/67/10/0	11	83	2	4	1.0

[a] Membranes were dark-adapted for 10 min and then given a series of 20 measuring flashes given at 4 Hz. Numerical analysis of the resultant amplitudes was performed using a four-state model as described previously (*43*, *59*)). [b] Oxygen release kinetics was estimated from the rising portion of the O_2 signal (Figure 4) using the exponential method as described previously (*60*).

exhibited relatively slow O_2 release kinetics indicative of a slowed S_3-S_0 transition, whereas O_2 release was unaffected in D1−D170H in D1−D170V membranes. These results are consistent with previous analysis of these mutants in terms of the estimated concentrations of Mn-containing centers versus their maximal rates of O_2-evolution. The previous estimates also suggest that the catalytic turnover rate is slower in D1−D170E than either D1−D170H or D1−D170V (*44*, *46*), consistent with the present interpretation that D1−D170E has the most impaired S_3-S_0 transition.

DISCUSSION

The primary event in the multistep photoassembly of the Mn_4−Ca cluster involves the binding and photooxidation of a single Mn^{2+} ion at the high affinity site of the apo-WOC (*22*, *23*). Mutational analysis has identified D1−D170 as a crucial residue of the high affinity site and essential for the efficient binding and photooxidation of the first Mn^{2+} involved in Mn_4−Ca assembly (*31*, *44*, *46*, *51*, *52*). The Michaelis constant of binding and photooxidation of Mn^{2+} in PSII core apo-complex has been quantitatively evaluated and shown to be dramatically altered by a variety of substitution mutations of D1−D170, including D1−D170A which does not allow assembly (*31*). Mutations of other residues in the same structural vicinity also strongly impact the high affinity site (*32*), but the disruptions in affinity are generally not as severe as for mutations at D1−D170. A handful of substitution mutations at D1−D170 permit the assembly of Mn clusters that evolve O_2. For this discussion, we assume that Mn_4−Ca is formed in the mutants, but that has not been definitely established, though spectroscopic analysis suggest this may be the case for D1−D170H (*53*, *54*). Decreased Mn^{2+} oxidation capacities, albeit still high enough to sustain assembly of Mn_4−Ca and O_2-evolution (*31*, *35*), are observed for the D1−D170E and D1−D170H mutants, which are subjects of the present study. The D1−D170E and D1−D170H mutants have roughly 2- and 10-fold higher K_M values, respectively, for Mn^{2+} at the high affinity site compared to the wild-type (*31*, *35*). The binding and photooxidation of Mn^{2+} in PSII core apo-complex has not yet been quantitatively evaluated in D1−D170V, the third mutant examined here. However, because the strain has a comparatively lower fraction of PSII containing functional Mn (*46*) and since the aliphatic nature of this side chain makes it an unlikely ligand of Mn (perhaps water serves this role in the mutant (*46*)), it seems probable that its capacity for Mn^{2+} binding and photooxidation is impaired.

Each of the three high affinity site mutants, D1−D170E, D1−D170H, and D1−D170V, exhibited impaired photoactivation kinetics, although each was unique in regard to the specific nature of the alterations in kinetics the mutation caused. The D1−D170H and D1−D170V mutants were prone to reversible photoinactivation yet exhibited nearly normal or even enhanced stability characteristics of the labile photoactivation intermediates (Figure 3 and Table 1). In contrast, photoactivation intermediates were highly destabilized by the D1−D170E mutation: it had optimum flash interval of approximately 200 ms, as opposed to the normal 500−1000 ms optimum in the control and the other mutants (Figure 3). This is consistent with the numerical analysis

assuming the PSII centers in D1−D170E are heterogeneous with respect to photoactivation kinetics and that the majority of centers are characterized by intermediates that decay ~10-fold more rapidly than the control (Figure 3, Table 1). This decreased stability of the intermediates is consistent with the very low quantum efficiency of photoactivation in the D1−D170E mutant, which is estimated to be less than 20% of the control based upon the slope of the curve of photoactivation as a function of flash number (Figure 2B). The result is superficially similar to the effect of the addition of exogenous reductant on the flash interval dependence of photoactivation, which likewise causes a decrease in the lifetime of assembly intermediates and shifts the optimum to shorter flash intervals (*26*): both the reductant and the mutation D1−D170E exhibit higher intermediate decay rate constants, k_D. As discussed previously, the first intermediate **B** (series two-quantum model shown in Scheme 1) is not likely to be rate-limiting (*13*, *17*, *25*, *26*). Instead, factors affecting the steady-state concentration and photoconversion of **C** govern the rate (and yield) of photoactivation (*13*, *17*, *25*, *26*). These factors can, in principle, include the rate of conversion of **B** to **C**, the stability of intermediate **C**, and the quantum efficiency of **C** ⟹ **D**. The conversion of **B** to **C** is slowed in D1−D170E, but it is also slowed in the other two mutants (Table 1), which do not exhibit lower overall quantum efficiencies of photoactivation. Therefore, the elevated decay rate, k_D, in D1−D170E seems to exclusively account for the low quantum efficiency of photoactivation in this mutant.

In contrast to D1−D170E, neither the quantum efficiency of photoactivation nor the stability of intermediates are diminished in D1−D170H and D1−D170V. However, flash photoactivation of D1−D170H and especially D1−D170V allowed recovery of only 50−60% of the original activity (Figure 2 and 4) and was the result of the accumulation of a correspondingly large percentage (40−50%) of inactive PSII centers. Furthermore, it was shown that most of the centers accumulating as inactive under flash illumination could be converted to apo-centers by re-extraction with HA and nearly fully photoactivated under continuous light hence the inactivation was reversible (Figure 4). The basis for low yields of photoactivation has been previously discussed in terms of three types of damage: (1) damage during extraction of Mn, (2) photoinhibition as defined as the light-induced loss of primary electron transport, and (3) photoinactivation defined as the light-induced loss of photoactivation without the loss of primary electron transport (*13*). The reversibility of the inactivation by reductive re-extraction with HA in the high affinity site mutants is consistent with the third type of damage and appears similar, as discussed below, to inactivation due to 'inappropriate' ligation of Mn (*50*, *55*). The nonproductive photoinactivation and the productive photoactivation pathways can be viewed as competing for the same pool of unactivated apo-PSII centers, and the ratio of the corresponding rates or probabilities determines the branching ratio of the alternative pathways and, ultimately, the final proportions of inactive and active centers that are yielded (*13*). Indeed, the shape of the curves in the photoactivation, especially in D1−D170V, as a function of flash number show an early saturation of PSII centers available for photoactivation consistent with this model of competition between the productive and nonproductive pathways. Placed in this context, the branching ratio between the nonproductive and productive pathways appears strongly influenced by the perturbation of the high affinity site. The difference between photoactivation under flash illumination versus continuous illumination is striking but remains to be understood. A reasonable hypothesis is that the difference is related to the degree occupancy of Mn at the high affinity site under these contrasting light regimes. Different illumination regimes have been previously supposed to give rise differences in the local concentration of Mn^{2+} in the vicinity of the high affinity site because of illumination differences to account for differences in fluorescence decay kinetics in *Synechocystis* PSII mutants (*56*). Differences in the kinetics of fluorescence decay in the *Synechocystis* PSII mutant, D1−S345P, were observed depending on whether the measurements were performed using a PAM fluorometer (*56*) or a pump−probe fluorometer (*56*, *57*). Higher occupancy of the high affinity site by Mn^{2+} was inferred when the PAM fluorometer was used. The modulated probe light of the PAM instrument has a considerable actinic effect under the conditions employed whereas the brief measuring light pulses of the pump−probe fluorometer used in the initial study have essentially no actinic effect (*56*, *57*). The actinic effect of the modulated probe light of the PAM fluorometer was thus proposed to increase the local concentration of Mn^{2+} in the vicinity of the high affinity site thereby increasing the occupancy by Mn^{2+} (*56*). By analogy, it appears that the differences between photoactivation under flash illumination and continuous illumination may relate to differences in local concentration of Mn^{2+} in the vicinity of the high affinity Mn site under these two illumination regimes with the local availability of Mn^{2+} being higher under continuous light. Thus, we tentatively conclude that the occupancy of the high affinity site determines whether or not the assembly path follows the functional or nonfunctional pathway.

The observation of reversible photoinactivation is reminiscent of previous results showing that Mn is photoligated 'inappropriately' as nonfunctional Mn under certain nonoptimal conditions *in vitro* (*50*, *55*). Photoactivation in the absence of Ca^{2+} resulted in the photoligation of up to eight Mn atoms per PSII, but these 'inappropriately bound', nonfunctional $Mn^{\geq 3+}$ were highly labile since they were reductively dissociated from PSII (*50*). Furthermore, photoinactivated PSII prepared by photoactivation in the absence of Ca^{2+} could be re-extracted with HA and subsequently photoactivated to produce high yields of O_2-evolving centers if the second photoactivation was performed in the presence of optimal concentrations of Ca^{2+} and Mn^{2+} (*50*). In this context, how would a mutation at the high affinity site tilt the branching ratio away from productive photoassembly and toward photoinactivation? One possibility is that the mutations not only affect the binding of Mn^{2+} but also perturb the Ca^{2+} site. Current crystallographic models do not place D1−D170 as a ligand of Ca^{2+} (*1*−*4*), which is consistent with the growth characteristics of mutants in Ca^{2+}-depleted media (*46*). On the other hand, several different mutations distributed at various locations around the overall coordination environment of the Mn_4−Ca were recently shown to affect the initial Mn^{2+} binding and photooxidation at the high affinity site in apo-PSII (*32*). Given the apparent interactions between locations in the coordination environment, it is not unreasonable that the D1−D170 mutants may also affect

Ca^{2+} binding, perhaps through electrostatic effects or second ligation sphere interactions. This possibility is consistent with recent findings that Ca^{2+} modifies the parallel mode EPR signal (*35*) of the first Mn photooxidation intermediate (*58*). It was shown that in the absence of Ca^{2+} or at low pH, an EPR-silent species of Mn^{3+} was generated by illumination of frozen samples, whereas Ca^{2+} or high pH favored a configuration giving rise to a parallel mode EPR signal. It was concluded that Ca^{2+} induces a structural change giving a single photogenerated Mn^{3+} and a less heterogeneous coordination environment, and this Ca^{2+}-induced structural change is associated with a deprotonation of a $Mn-H_2O$ ligand, perhaps bridging with the Ca^{2+} at its effector site. Considering the formation of inappropriately bound $Mn^{\geq 3+}$ depending on the absence of Ca^{2+} during photoactivation (*50*, *55*), the EPR-silent species of Mn^{3+} in the absence of Ca^{2+} might correspond to a structural configuration conducive to the addition of inappropriately bound, nonfunctional $Mn^{\geq 3+}$. Thus, Ca^{2+} may serve to organize the coordination environment that promotes photooxidation of Mn^{2+} in a structural configuration, promoting subsequent Mn assembly into a functional WOC and discouraging entry of that center into the photoinactivation pathway. Placed in this context, a speculative interpretation of the current results is that the D1−D170H and D1−D170V mutations not only disturb Mn^{2+} photooxidation at the high affinity site but also disturb this optimal Ca^{2+}-induced configuration and allow a greater fraction of centers to enter the nonproductive pathway where photooxidation of Mn^{2+} at the inappropriate site(s) can occur readily.

ACKNOWLEDGMENT

Insightful contributions of the reviewers are acknowledged including the strategy for quantitative analysis of heterogeneous populations of centers, which was developed by an anonymous reviewer.

REFERENCES

1. Ferreira, K. N., Iverson, T. M., Maghlaoui, K., Barber, J., and Iwata, S. (2004) Architecture of the photosynthetic oxygen-evolving center, *Science 303*, 1831−1838.
2. Kamiya, N., and Shen, J. R. (2003) Crystal structure of oxygen-evolving photosystem II from Thermosynechococcus vulcanus at 3.7-Å resolution, *Proc. Natl. Acad. Sci. U.S.A. 100*, 98−103.
3. Loll, B., Kern, J., Saenger, W., Zouni, A., and Biesiadka, J. (2005) Towards complete cofactor arrangement in the 3.0 Å resolution structure of photosystem II, *Nature 438*, 1040−1044.
4. Zouni, A., Witt, H. T., Kern, J., Fromme, P., Krauss, N., Saenger, W., and Orth, P. (2001) Crystal structure of photosystem II from *Synechococcus elongatus* at 3.8 Å resolution, *Nature 409*, 739−743.
5. Ono, T. (2001) Metallo-radical hypothesis for photoassembly of $(Mn)_4$-cluster of photosynthetic oxygen evolving complex, *Biochim. Biophys. Acta 1503*, 40−51.
6. Burnap, R. L. (2004) D1 protein processing and Mn cluster assembly in light of the emerging photosystem II structure, *Phys. Chem. Chem. Phys. 6*, 4803−4809.
7. Cheniae, G. M., and Martin, I. F. (1971) Photoactivation of the manganese catalyst of O_2 evolution. I. Biochemical and kinetic aspects, *Biochim. Biophys. Acta 253*, 167−181.
8. Cheniae, G. M., and Martin, I. F. (1971) Effects of hydroxylamine on photosystem II. I. Factors affecting the decay of O_2 evolution, *Plant Physiol. 47*, 568−575.
9. Hwang, H. J., and Burnap, R. L. (2005) Multiflash experiments reveal a new kinetic phase of photosystem II manganese cluster assembly in *Synechocystis* sp PCC6803 in vivo, *Biochemistry 44*, 9766−9774.
10. Tamura, N., and Cheniae, G. (1987) Photoactivation of the water-oxidizing complex in photosystem II membranes depleted of Mn and extrinsic proteins. I. Biochemical and kinetic characterization, *Biochim. Biophys. Acta 890*, 179−194.
11. Cheniae, G. M., and Martin, I. F. (1972) Effects of hydroxylamine on photosystem II. II Photoreversal of the NH_2OH destruction of O_2 evolution, *Plant Physiol. 50*, 87−94.
12. Radmer, R., and Cheniae, G. M. (1971) Photoactivation of the manganese catalyst of O_2 evolution. II. A two quantum mechanism, *Biochim. Biophys. Acta 253*, 182−186.
13. Miller, A. F., and Brudvig, G. W. (1989) Manganese and Calcium Requirements for Reconstitution of Oxygen-Evolution Activity in Manganese-Depleted Photosystem-II Membranes, *Biochemistry 28*, 8181−8190.
14. Miyao, M., and Inoue, Y. (1991) An improved procedure for the photoactivation of photosynthetic oxygen evolution: Effect of artificial electron acceptors on the photoactivation yield of NH_2-OH-treated wheat photosystem II membranes, *Biochim. Biophys. Acta 1056*, 47−56.
15. Miyao, Tokutomi, M., and Inoue, Y. (1992) Improvement by benzoquinones of the quantum yield of photoactivation of photosynthetic oxygen evolution: direct evidence for the two quantum mechanism, *Biochemistry 31*, 526−532.
16. Burnap, R. L., Qian, M., Al-Khaldi, S., and Pierce, C. (1995) Photoactivation and S-state cycling kinetics in photosystem II mutants in *Synechocystis* sp. PCC6803, in *Photosynthesis: from light to biosphere* (Mathis, P., Ed.) pp 443−446, Kluwer Academic Publishers, Dordrect, The Netherlands.
17. Burnap, R. L., Qian, M., and Pierce, C. (1996) The manganese-stabilizing protein (MSP) of photosystem II modifies the *in vivo* deactivation and photoactivation kinetics of the H_2O-oxidation complex in *Synechocystis* sp. PCC6803, *Biochemistry 35*, 874−882.
18. Ananyev, G. M., and Dismukes, G. C. (1996) High resolution kinetic studies of the reassembly of the tetra manganese cluster of photosynthetic water oxidation: proton equilibrium, cations, and electrostatics, *Biochemistry 35*, 14608−14617.
19. Zaltsman, L., Ananyev, G. M., Bruntrager, E., and Dismukes, G. C. (1997) Quantitative kinetic model for photoassembly of the photosynthetic water oxidase from its inorganic constituents: requirements for manganese and calcium in the kinetically resolved steps, *Biochemistry 36*, 8914−8922.
20. Barra, M., Haumann, M., Loja, P., Krivanek, R., Grundmeier, A., and Dau, H. (2006) Intermediates in assembly by photoactivation after thermally accelerated disassembly of the manganese complex of photosynthetic water oxidation, *Biochemistry 45*, 14523−14532.
21. Riggs, P. J., Mei, R., Yocum, C. F., and Penner, H. J. E. (1992) Reduced derivatives of the manganese cluster in the photosynthetic oxygen-evolving complex, *J. Am. Chem. Soc. 114*, 10650−10651.
22. Ono, T. A., and Mino, H. (1999) Unique binding site for Mn^{2+} ion responsible for reducing an oxidized Y_Z tyrosine in manganese-depleted photosystem II membranes, *Biochemistry 38*, 8778−8785.
23. Ananyev, G. M., Murphy, A., Abe, Y., and Dismukes, G. C. (1999) Remarkable affinity and selectivity for Cs^+ and uranyl (UO_2^{2+}) binding to the manganese site of the apo-water oxidation complex of photosystem II, *Biochemistry 38*, 7200−7209.
24. Ananyev, G. M., Zaltsman, L., Vasko, C., and Dismukes, G. C. (2001) The inorganic biochemistry of photosynthetic oxygen evolution/water oxidation, *Biochim. Biophys. Acta 1503*, 52−68.
25. Ananyev, G. M., and Dismukes, G. C. (1996) Assembly of the tetra Mn site of photosynthetic water oxidation by photoactivation: Mn stoichiometry and detection of a new intermediate, *Biochemistry 35*, 4102−4109.
26. Ono, T. A., and Inoue, Y. (1987) Reductant-sensitive intermediates involved in multi-quantum process of photoactivation of latent oxygen-evolving system, *Plant Cell Physiol. 28*, 1293−1300.
27. Hoganson, C. W., Ghanotakis, D. F., Babcock, G. T., and Yocum, C. F. (1989) Manganese ion reduces redox activated tyrosine in manganese-depleted photosystem II preparations, *Photosynth. Res. 22*, 285−294.
28. Diner, B. A., and Nixon, P. J. (1992) The Rate of Reduction of Oxidized Redox-Active Tyrosine, Z^+, by Exogenous Mn^{2+} Is Slowed in a Site-Directed Mutant, at Aspartate 170 of Polypeptide D1 of Photosystem-II, Inactive for Photosynthetic Oxygen Evolution, *Biochim. Biophys. Acta 1101*, 134−138.
29. Ahlbrink, R., Semin, B. K., Mulkidjanian, A. Y., and Junge, W. (2001) Photosystem II of peas: effects of added divalent cations of Mn, Fe, Mg, and Ca on two kinetic components of $P^{(+)}_{(680)}$

reduction in Mn-depleted core particles, *Biochim. Biophys. Acta 1506*, 117−126.
30. Boerner, R. J., Nguyen, A. P., Barry, B. A., and Debus, R. J. (1992) Evidence from directed mutagenesis that aspartate 170 of the D1 polypeptide influences the assembly and/or stability of the manganese cluster in the photosynthetic water-splitting complex, *Biochemistry 31*, 6660−6672.
31. Nixon, P. J., and Diner, B. A. (1992) Aspartate 170 of the photosystem II reaction center polypeptide D1 is involved in the assembly of the oxygen evolving manganese cluster, *Biochemistry 31*, 942−948.
32. Cohen, R. O., Nixon, P. J., and Diner, B. A. (2007) Participation of the C-terminal region of the D1-polypeptide in the first steps in the assembly of the Mn_4Ca cluster of photosystem II, *J. Biol. Chem. 282*, 7209−7218.
33. Chu, H. A., Nguyen, A. P., and Debus, R. J. (1995) Amino acid residues that influence the binding of manganese or calcium to photosystem II. 2. The carboxy terminal domain of the D1 polypeptide, *Biochemistry 34*, 5859−5882.
34. Nixon, P. J., Chisholm, D. A., and Diner, B. A. (1992) Isolation and functional analysis of random and site-directed mutants of photosystem II, in *Plant Microbial Biotechnology Research Series* (Shewry, P. R., and Gutteridge, S., Eds.), pp 93−141, Cambridge University Press, Cambridge, U.K.
35. Campbell, K. A., Force, D. A., Nixon, P. J., Dole, F., Diner, B. A., and Britt, R. D. (2000) Dual-Mode EPR Detects the Initial Intermediate in Photoassembly of the Photosystem II Mn Cluster: The Influence of Amino Acid Residue 170 of the D1 Polypeptide on Mn Coordination, *Biochemistry 122*, 3754−3761.
36. Williams, J. G. K. (1988) Construction of specific mutations in Photosystem II photosynthetic reaction center by genetic engineering methods in Synechocystis 6803, *Methods Enzymol. 167*, 766−778.
37. Li, Z. L., and Burnap, R. L. (2002) Mutations of basic arginine residue 334 in the D1 protein of Photosystem II lead to unusual S_2 state properties in Synechocystis sp PCC 6803, *Photosynth. Res. 72*, 191−201.
38. Qian, M., Dao, L., Debus, R. J., and Burnap, R. L. (1999) Impact of mutations within the putative Ca^{2+}-binding lumenal interhelical a-b loop of the photosystem II D1 protein on the kinetics of photoactivation and H_2O-oxidation in *Synechocystis* sp. PCC6803, *Biochemistry 38*, 6070−6081.
39. Lavorel, J. (1992) Determination of the photosynthetic oxygen release time by amperometry, *Biochim. Biophys. Acta 1101*, 33−40.
40. Miyao, M., Murata, N., Lavorel, J., Maison-peteri, B., Boussac, A., and Etienne, A.-L. (1987) Effect of the 33-kDa protein on the S-state transitions in photosynthetic oxygen evolution., *Biochim. Biophys. Acta 890*, 151−159.
41. Meunier, P. C., and Popovic, R. (1991) The time for oxygen release in photosynthesis: Reconciliation of flash polarography with other measurement techniques., *Photosynth. Res. 28*, 33−39.
42. Clausen, J., Debus, R. J., and Junge, W. (2004) Time-resolved oxygen production by PSII: chasing chemical intermediates, *Biochim. Biophys. Acta 1655*, 184−194.
43. Meunier, P. C., Burnap, R. L., and Sherman, L. A. (1995) Modelling of the S-state mechanism and Photosystem II manganese photoactivation in cyanobacteria, *Photosynth. Res. 47*, 61−76.
44. Chu, H.-A., Nguyen, A. P., and Debus, R. A. (1994) Site-directed mutagenesis of photosynthetic oxygen evolution: Instability or inefficient assembly of the manganese cluster *in vivo*., *Biochemistry 33*, 6137−6149.
45. Debus, R. A., Nguyen, A. P., and Conway, A. B. (1990) Identification of ligands to manganese and calcium in photosystem II by site-directed mutagensis., in *Current Research in Photosynthesis* (Baltscheffsky, M., Ed.), pp 829−832, Kluwer, Dordrecht, The Netherlands.
46. Chu, H. A., Nguyen, A. P., and Debus, R. J. (1995) Amino acid residues that influence the binding of manganese or calcium to photosystem II. 1. The lumenal interhelical domains of the D1 polypeptide, *Biochemistry 34*, 5839−5858.
47. Debus, R. J., Campbell, K. A., Gregor, W., Li, Z. L., Burnap, R. L., and Britt, R. D. (2001) Does histidine 332 of the D1 polypeptide ligate the manganese cluster in photosystem II? An electron spin echo envelope modulation study, *Biochemistry 40*, 3690−3699.
48. Qian, M., Al Khaldi, S. F., Putnam Evans, C., Bricker, T. M., and Burnap, R. L. (1997) Photoassembly of the photosystem II Mn_4 cluster in site directed mutants impaired in the binding of the manganese stabilizing protein, *Biochemistry 36*, 15244−15252.
49. Li, Z. L., and Burnap, R. L. (2001) Mutations of arginine 64 within the putative Ca^{2+}-binding lumenal interhelical a-b loop of the photosystem II D1 protein disrupt binding of the manganese stabilizing protein and cytochrome c_{550} in *Synechocystis* sp. PCC6803, *Biochemistry 40*, 10350−10359.
50. Chen, C., Kazimir, J., and Cheniae, G. M. (1995) Calcium modulates the photoassembly of photosystem II $(Mn)_4$ clusters by preventing ligation of nonfunctional high valency states of manganese, *Biochemistry 34*, 13511−13526.
51. Boerner, R. J., Bixby, K. A., Nguyen, A. P., Noren, G. H., Debus, R. J., and Barry, B. A. (1993) Removal of stable tyrosine radical D^+ affects the structure or redox properties of tyrosine z in manganese-depleted photosystem ii particles from synechocystis 6803, *J. Biol. Chem. 268*, 1817−1823.
52. Nixon, P. J., and Diner, B. A. (1994) Analysis of water oxidation mutants constructed in the cyanobacterium Synechocystis sp. PCC 6803, *Biochem. Soc. Trans.* 22, 338−343.
53. Debus, R. J., Aznar, C., Campbell, K. A., Gregor, W., Diner, B. A., and Britt, R. D. (2003) Does aspartate 170 of the D1 polypeptide ligate the manganese cluster in photosystem II? An EPR and ESEEM study, *Biochemistry 42*, 10600−10608.
54. Chu, H. A., Debus, R. J., and Babcock, G. T. (2001) D1-asp170 is structurally coupled to the oxygen evolving complex in photosystem II as revealed by light-induced fourier transform infrared difference spectroscopy, *Biochemistry 40*, 2312−2316.
55. Tamura, N., Inoue, Y., and Cheniae, G. (1989) Photoactivation of the water-oxidizing complex in photosystem II membranes depleted of Mn, Ca, and extrinsic proteins. II. Studies on the function of Ca^{2+}. *Biochim. Biophys. Acta 976*, 173−181.
56. Chu, H.-A., Nguyen, A. P., and Debus, R. A. (1994) Site-directed mutagenesis of photosynthetic oxygen evolution: Increased binding or photooxidation of manganese in the absence of the extrinsic 33-kDa polypeptide *in vivo*, *Biochemistry 33*, 6150−6157.
57. Nixon, P. J., Trost, J. T., and Diner, B. A. (1992) Role of the carboxy terminus of polypeptide D1 in the assembly of a functional water oxidizing manganese cluster in photosystem II of the cyanobacterium *Synechocystis* sp. PCC 6803: assembly requires a free carboxyl group at C terminal position 344, *Biochemistry 31*, 10859−10871.
58. Tyryshkin, A. M., Watt, R. K., Baranov, S. V., Dasgupta, J., Hendrich, M. P., and Dismukes, G. C. (2006) Spectroscopic evidence for Ca^{2+} involvement in the assembly of the Mn_4Ca cluster in the photosynthetic water-oxidizing complex, *Biochemistry 45*, 12876−12889.
59. Lavorel, J. (1976) Matrix analysis of the oxygen evolving system of photosynthesis, *J. Theor. Biol 57*, 171−185.
60. Jursinic, P. A., and Dennenberg, R. J. (1990) Oxygen release time in leaf discs and thylakoids of peas and Photosystem II membrane fragments of Spinach, *Biochim. Biophys. Acta 1020*, 195−206.

BI700761V